MARFit: An Integrated Software for Real-Time MR Guided Focused Ultrasound Neuromodulation System

Yangzi Qiao, Chao Zou, Jianhong Wen, Xiaojing Long, Chuanli Cheng, Wanqun Yang, Weitao Ye, Dong Liang, *Senior Member, IEEE*, Xin Liu, and Hairong Zheng, *Senior Member, IEEE*

***Abstract*— MR guided focused ultrasound (MRgFUS) therapy has been a promising treatment modality for many neurological disorders. However, the lack of real-time image processing software platform sets barriers for relevant pre-clinical researches. This work intends to develop an integrated software for MRgFUS therapy. The software contains three functional modules: a communication module, an image post-processing module, and a visualization module. The communication module provides a data interface with an open-source MR image reconstruction platform (Gadgetron) to receive the reconstructed MR images in real-time. The post-processing module contains the algorithms of image coordinate registration, focus localization by MR acoustic radiation force imaging (MR-ARFI), temperature and thermal dose calculations, motion correction, and temperature feedback control. The visualization module displays monitoring information and provides a user-machine interface. The software was tested to be compatible with systems from two different vendors and validated in multiple scenarios for MRgFUS. The software was tested in many *ex vivo* and *in vivo* experiments to validate its functions. The *in vivo* transcranial focus localization experiments were carried out for targeting the focused ultrasound in neuromodulation.**

***Index Terms*— MR guided focused ultrasound (MRgFUS), Software, MR acoustic radiation force imaging (MR-ARFI), MR thermometry (MRT).**

Manuscript received July 15, 2021; revised December 9, 2021; accepted January 8, 2022. Date of publication January 25, 2022; date of current version February 9, 2022. This work was supported in part by the National Natural Science Foundation of China under Grant 81527901, in part by the Shenzhen Key Laboratory of Ultrasound Imaging and Therapy under Grant ZDSYS 201802061806314, in part by the Guangdong Grant for "Key Technologies for Treatment of Brain Disorders" under Grant 2018B030332001, in part by the Key Laboratory for Magnetic Resonance and Multimodality Imaging of Guangdong Province under Grant 2020B1212060051, in part by the Shenzhen Double Chain under Grant [2018] 256, in part by the Scientific Instrument Innovation Team of the Chinese Academy of Sciences under Grant GJJSTD20180002, in part by the International Partnership Program of Chinese Academy of Sciences under Grant 154144KYSB20180063, and in part by the National Science Foundation for Young Scientists of China under Grant 81701662. *(Corresponding author: Chao Zou.)*

This work involved human subjects or animals in its research. Approval of all ethical and experimental procedures and protocols was granted by the Institutional Ethical Committee of the Shenzhen Institutes of Advanced Technology, Chinese Academy of Sciences under IACUC Protocol Nos. SIAT-IRB-200315-H0454, and original: SIAT-IRB-170425-YGS-ZHR-A0094-2 and amended: SIAT-IACUC-200417-YB-ZHR-A0094-2-04.

Yangzi Qiao, Chao Zou, Xiaojing Long, Chuanli Cheng, Dong Liang, Xin Liu, and Hairong Zheng are with the Paul C. Lauterbur Research Center for Biomedical Imaging, Shenzhen Institutes of Advanced Technology, Chinese Academy of Sciences, Shenzhen 518055, China (e-mail: yz.qiao@siat.ac.cn; chao.zou@siat.ac.cn; xj.long@siat.ac.cn; cl.cheng@siat.ac.cn; dong.liang@siat.ac.cn; xin.liu@siat.ac.cn; hr.zheng@siat.ac.cn).

Jianhong Wen is with Zhongke Green Valley (Shenzhen) Medical Technology Company Ltd., Shenzhen 518055, China (e-mail: wenjianhong@mail.gvbraintech.com).

Wanqun Yang and Weitao Ye are with Guangdong Provincial People's Hospital, Guangdong Academy of Medical Sciences, Guangzhou 510000, China (e-mail: yingxiangwanqun@163.com; wuchuanywt@qq.com).

This article has supplementary downloadable material available at https://doi.org/10.1109/TNSRE.2022.3146286, provided by the authors.

Digital Object Identifier 10.1109/TNSRE.2022.3146286

I. Introduction

MR GUIDED focused ultrasound (MRgFUS) therapy has been a promising treatment modality for many neurological disorders, such as essential tremor [1], Parkinson's disease [2], Alzheimer disease [3] etc. MR plays a crucial role in nearly every step of FUS therapy, from treatment planning to real-time monitoring, and treatment assessment. MRgFUS demands faster image acquisition, reconstruction, and post-processing compared to diagnostic MR imaging. The anatomical images and processed monitoring information should be visualized with minimum latency for real-time guidance. Automatic adjustment of FUS parameters combined with safety concerns is also indispensable. All these specific requirements raise the need for a dedicated, extensible MRgFUS software platform.

There have already been some powerful commercial MRgFUS platforms, include the software component of ExAblate Neuro (Insightec, Haifa, Israel), TULSA-PRO (Profound Medical Inc., Toronto, Canada), Sonalleve MR-HIFU (Philips Healthcare, Vantaa, Finland) etc. However, these commercial software are too expensive for pre-clinical studies, and are compatible with a limited number of MR systems. To translate the platform between different vendors involves addressing complicated financial interests and regulatory restrictions, which urges many groups to carry out MRgFUS studies based on a third party software [4]–[8].

Thermoguide (Image guided therapy, Pessac, France) and RTHawk (HeartVista, Los Altos, CA) are the two most commonly used third party softwares. Thermoguide has features of compatibility with different vendor's MR host, arbitrary trajectory planning, and robust temperature measurement. With the help of Thermoguide, Fite *et al.* developed an MRgFUS system with the automatic thermal dose controlled by proportional integral derivative (PID) algorithm [4]. Magnin *et al.* carried out an MR guided blood-brain barrier opening experiment with programmed trajectories [5]. Liu *et al.* visualized the acoustic radiation force induced displacement and shear wave propagation concurrently with temperature monitoring [6]. RTHawk is a commercial software developed for real-time cardiac imaging [7]. However, it is also compatible with MRgFUS. Combined with Vurtigo visualization [8], the extensible platform enables researchers to create pulse sequences, process the data in real-time and change the imaging parameters at any time [9]. Despite the powerful functions, Thermoguide and RTHawk are still quite expensive.

Smink *et al.* have developed a flexible scanner interface, eXTernal Control (XTC), which can communicate directly with the Philips scanner [10]. The work on XTC was then leveraged by Zaporzan *et al.* to develop software toolboxes for real-time communication with Philips MRI scanner (MatMRI) and robust control of the Philips Sonalleve clinical MR-HIFU system (MatHIFU) in a MATLAB environment [11]. Rieck *et al.* carried out the first *in vivo* treatment of localized abscesses induced by methicillin-resistant staphylococcus aureus (MRSA) based on this platform [12]. Even though the software was intended to be freely available as open-source projects to other research groups, they are only friendly to the users of Philips Sonalleve MR-HIFU therapy system. Later, Pichardo *et al.* developed a new generation of the MRgFUS software platform Proteus [13]. This excellent software was aimed to facilitate the development of new therapeutic applications by providing a core of functionalities that are independent of MRI or MRI-HIFU vendors. However, it also goes commercial recently. Poorman *et al.* developed an open source small animal MRgFUS system and published their MATLAB code for pre-clinical research [14]. The software includes many essential functions of MRgFUS treatment and can trigger image post-processing directly after receiving the reconstructed images from the scanner. However, the software relies firmly on the availability of the reconstructed images from the scanner. Therefore, the accessibility of the raw data and the compatibility of newly developed reconstruction algorithm are challenging in some pre-clinical environments.

In this study, we developed an MRgFUS software named MARFit. It was written in C++ and build from several open-source libraries, including DICOM ToolKit (DCMTK), Armadillo and Visualization ToolKjit (VTK). The real-time image reconstruction and communication with the MRI system was based on Gadgetron, which is an open-source framework designed for medical image reconstruction [15]. The software covers various functions including the coordinate registration, ultrasound focal area localization based on acoustic radiation force imaging (ARFI), temperature measurement, thermal dose calculation, motion correction and temperature feedback control, which are fundamental for MRgFUS treatment. The software was first tested in many *ex vivo* and *in vivo* experiments to validate its functions. Then the *in vivo* transcranial focus localization experiment was carried out, which is the most appealing technique in targeting the focus ultrasound for use in neuromodulation [16]. The processed results provided accurate imaging guidance and monitoring information. Besides, it has good extensibility, flexibility, and translatability between MR systems from different vendors.

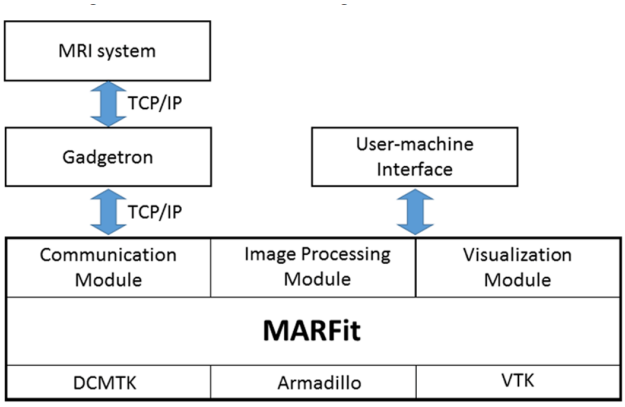

Fig. 1. The schematic design of the software.

II. Method

A. Software Architecture

MARFit consists of three functional modules. They are the Communication Module, Visualization Module and Image Processing Module, as shown in Fig. 1.

B. Communication Module

The Communication Module receives the reconstructed MR data from Gadgetron through TCP/IP. (The integration of Gadgetron with UIH and Siemens scanner are introduced in Appendix A of Supplementary Materials.) While collecting the data from Gadgetron, the communication module extracts the header information from the data, including the basic scanning parameters, patient information, imaging position, and orientation. The communication module then attaches the currently received data to a pre-defined tree structure and arranges the sequentially scanned data as a temporal series. Finally, the module translates the acquired complex images into the VTK data format, which incorporates the image position and orientation information for the final image processing and visualization.

The data streaming from the MR system to the communication module of MARFit is illustrated in Fig. 2. The sequence run in the MR systems needs to be slightly modified to enable the transmission of the k-space data to Gadgetron in a real-time way. In Gadgetron, several functional modules (called gadgets) were developed, organized, and finally explicitly configured as a data processing pipeline to the running sequences. Finally, the pipeline reconstructs the k-space data to the complex image after assembling several pieces of header information and then sends the image to MARFit. The processing pipeline for a

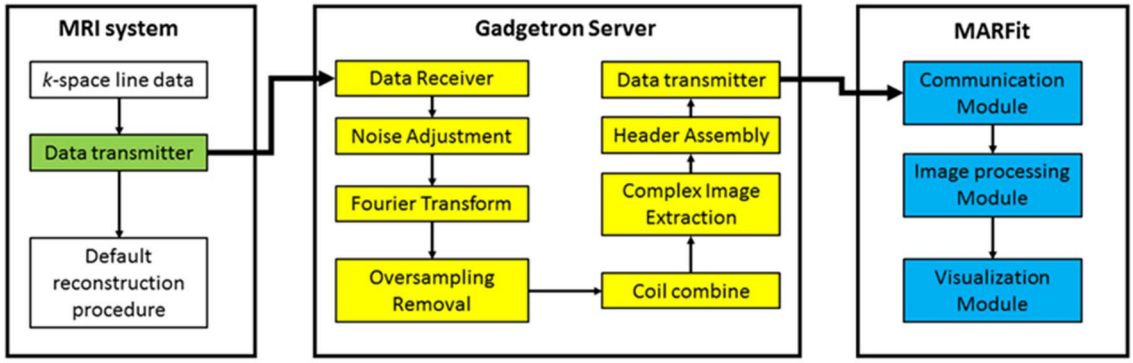

Fig. 2. MR data streaming.

simple GRE sequence with Cartesian sampling is illustrated in Fig. 2. The communication module is also compatible with the DICOM images from the MR reconstruction system directly through the DCMTK interface.

C. Image Processing Module

The Image Processing Module contains the algorithms of coordinate registration, acoustic radiation force imaging, temperature and thermal dose calculations, motion correction, and temperature control.

1) Coordinate Registration: There are typically three coordinate systems in MRgFUS systems: patient coordinate (P), ultrasound transducer coordinate (U), and MR image coordinate (I). Image registration aims to obtain the transformation matrices between P-, U- and I-coordinates so that the ultrasound focal location and propagation direction can be merged in the MR images visually for treatment planning.

The transformation matrix between P- and I- coordinates can be obtained from the sequence protocol extracted in the data header, which is transmitted through the Gadgetron pipeline and finally to MARFit along with the image data. The coordinates of image pixel (i, j) in P-Coordinate was calculated through:

$$\begin{bmatrix} P_x \\ P_y \\ P_z \\ 1 \end{bmatrix} = \begin{bmatrix} X\,cos_x\Delta_i & Y\,cos_x\Delta_j & 0 & O_x \\ X\,cos_y\Delta_i & Y\,cos_y\Delta_j & 0 & O_y \\ X\,cos_z\Delta_i & Y\,cos_z\Delta_j & 0 & O_z \\ 0 & 0 & 0 & 1 \end{bmatrix} \begin{bmatrix} i \\ j \\ 0 \\ 0 \end{bmatrix} \quad (1)$$

, where $O_{x,y,z}$ are the P-coordinates of the upper left image corner. $X\,\cos_{x,y,z}$, $Y\,\cos_{x,y,z}$ are the direction cosines of the first row and column in the P-Coordinate, Δ_i and Δ_j are the pixel resolutions in both directions.

The transformation matrix between the I- and the U-coordinate was obtained with the help of specially designed localizer balls, whose relative position to the transducer center was exactly known (coordinates in U-coordinate). The I-coordinates of the localizer balls were extracted from a pre-scanned high resolution heavily T1 weighted image. Based on image thresholding and Hough transformation (Fig. 3), the geometric centres of the localizer balls in the I-coordinates are fitted, and the rigid coordinate transformation matrix M_{U-I}

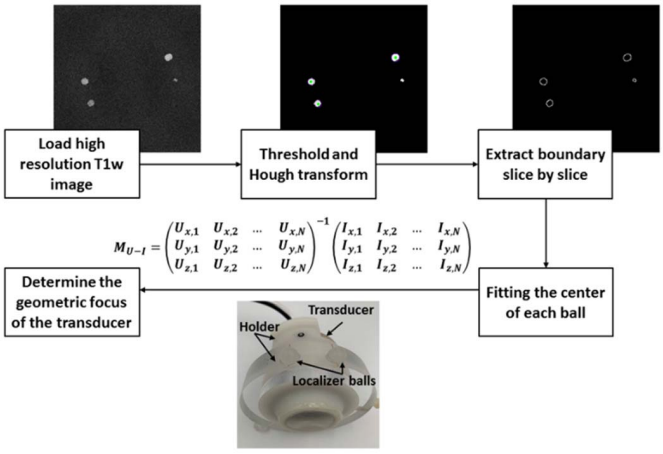

Fig. 3. Image registration between ultrasound transducer coordinate and MR image coordinate.

can be calculated by:

$$M_{U-I} = \begin{pmatrix} U_{x,1} & U_{x,2} & \cdots & U_{x,N} \\ U_{y,1} & U_{y,2} & \cdots & U_{y,N} \\ U_{z,1} & U_{z,2} & \cdots & U_{z,N} \end{pmatrix}^{-1} \times \begin{pmatrix} I_{x,1} & I_{x,2} & \cdots & I_{x,N} \\ I_{y,1} & I_{y,2} & \cdots & I_{y,N} \\ I_{z,1} & I_{z,2} & \cdots & I_{z,N} \end{pmatrix} \quad (2)$$

$I_{x,k}, I_{y,k}, I_{z,k}$ are the coordinates of the k-th ball's center in the I-Coordinate, while $U_{x,k}, U_{y,k}, U_{z,k}$ are the coordinates of the k-th ball's center in the U-Coordinate. The geometric focus and the ultrasound propagation direction of the transducer in the I-Coordinate can be determined based on the M_{U-I}.

2) MR-ARFI: MR acoustic radiation force imaging (MR-ARFI) is a feature integrated into the software to precisely localize the transcranial focus of the ultrasound with minimal temperature rise [17]. MR-ARFI helps in cases where the skull would significantly shift the ultrasound focus in transcranial applications. Though the geometric focus of the transducer can be obtained through the coordinate registration, the MR-ARFI feature aids in the actual focus localization when the ultrasound wave is distorted due to the sonic impedance mismatch in the tissue interface.

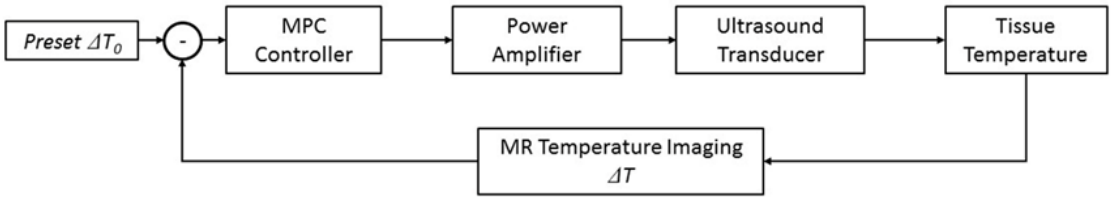

Fig. 4. Schematic design of the feedback temperature control.

Four displacement encoded images are required for the ultrasound-induced displacement calculation in the current implementation. Two complex images (with their phase images $\varphi^+$and φ^-) with the opposite polarities of displacement encoding gradient (DEG) were acquired during ultrasound pulse ON to increase the detection sensitivity [18]. Another two complex images (with their phase images φ^+_{ref} and φ^-_{ref}) without HIFU pulse were also needed to avoid the eddy current problem raised from inverted gradient polarities. All complex images were reconstructed in Gadgetron and sent to MARFit. The displacement was calculated by:

$$D = \frac{(\varphi^+ - \varphi^-) - (\varphi^+_{ref} - \varphi^-_{ref})}{2\gamma G\tau}, \tag{3}$$

where γ is the gyro-magnetic ratio. Based on the displacement map, the focus of the ultrasound would be automatically localized at the maximum displacement within the selected ROI.

3) Temperature Monitoring: Temperature monitoring is a unique feature which can be provided by MR imaging during FUS treatment. The proton resonance frequency shift (PRFS) method based on GRE sequence is the most common choice to generate the real-time temperature change maps. The temperature change $\Delta T(t)$ can be expressed as [19]:

$$\Delta T(t) = \frac{\varphi(t) - \varphi_{ref}}{\gamma\,\alpha B_0 T E}, \tag{4}$$

where α is the PRFS coefficient to temperature, $\varphi(t)$ is the phase image at time t and φ_{ref} is the reference phase image before the temperature change occurred.

The thermal dose information was also integrated into the software based on the following equation:

$$CEM43°C = \sum_{i=1}^{n} R^{(43-T_i)}\Delta t \tag{5}$$

where $CEM43°C$ is the equivalent time at 43°C [20], T_i is the temperature during i-th time interval Δt, R=0.5 above 43° C, and R = 0.25 below 42°C.

4) Motion Correction: The PRFS temperature mapping method is intrinsically vulnerable to motion as it is based on the reference image acquisition. Recently, many motion correction methods [21]–[25] have been proposed to address this problem. In our software, both multiple reference method and referenceless method have been implemented and integrated into the image post-processing module. For the multi-reference phase correction, a reference atlas of N images without heating was acquired first. The dynamic reference images were generated based on the principal component analysis (PCA) method [24]. For the referenceless method, the phase finite difference method [25] has been realized. These methods can be chosen manually in the user-machine interface. The full explanations of the multiple reference and referenceless methods are provided in Appendix B of Supplementary Materials.

5) Temperature Control: Elevating tissue temperature to a mild 42°C and maintaining for a short period of time has been termed as hyperthermia, which can increase blood flow and drug absorption in the targeted region without causing permanent damage. A real-time temperature feedback control algorithm was implemented to realize temperature control at the target value. To be adaptive to different tissues and reduce the reliability of parameter-tunning, model predictive control (MPC) algorithm was adopted based on auto regressive and moving average (ARMA) model. In this algorithm, the temperature change of the tissue in the future frames was predicted, and the temperature change model was modified online promptly. The goal of the MPC controller was to achieve the target value of the temperature as soon as possible and avoid severe overshoot. The controller outputs a signal amplitude value to a sine signal with the oscillating frequency equal to the resonance frequency of the ultrasound transducer. The sine signal was then amplified to drive the ultrasound transducer. The detail of the MPC algorithm is given in Appendix C of Supplementary Materials.

D. Visualization Module

The Visualization Module provides the user-machine interface and image rendering, as shown in Fig. 5. Real-time images are organized in a tree structure and displayed in the left tab-view. The sequential images are attached as leaf nodes. In the image visualization window, the temperature map can be merged with anatomical images. The temperature change curve of any pixel was observed in the upper-right corner window. The lower-left corner window displays the thermal dose map or MR-ARFI map according to the user's choice. In Fig. 5, a transcranial MR-ARFI result was shown in the illustration. Other settings such as ROI selection, algorithms for motion correction, and thermal control were all integrated into separate tab-views in the lower-right window.

III. Experiments

MARFit was run on a workstation (Intel i7-4800MQ CPU, 16GB RAM). The MR image reconstruction was implemented

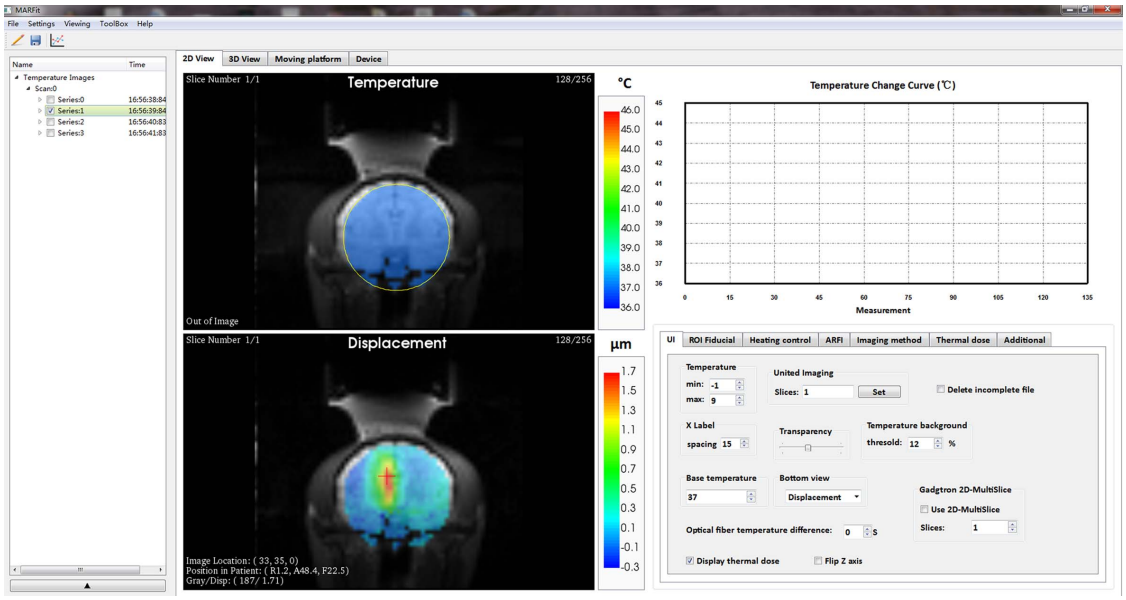

Fig. 5. The user interface of the software.

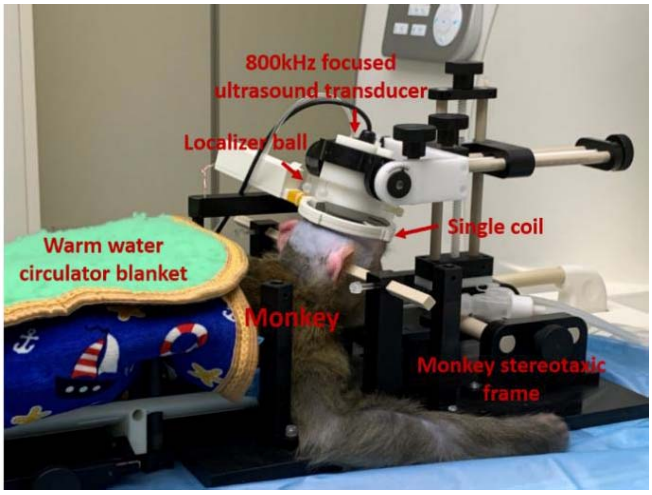

Fig. 6. System set-up of *in vivo* MR-ARFI.

in a Gadgetron server, which was equipped with Intel E5-2698v4 CPU, 128GB RAM with Gadgetron version 3.12.0.

The informed consent was received from all the human volunteers. All the volunteer and animal experiments were reviewed and approved by the local institutional review board (no. SIAT-IRB-200315-H0454, and no. original-SIAT-IRB-170425-YGS-ZHR-A0094-2, amended-SIAT-IACUC-200417-YB-ZHR-A0094-2-04).

A. MRI and Ultrasound Equipment

All the functions of the software were validated in two systems, the UIH 3.0T system (uMR790, Shanghai United Imaging Healthcare, Shanghai, China) and the Siemens 3T system (Siemens TIM TRIO, Erlangen, Germany) except for the transcranial MR-ARFI. The experiments for transcranial MR-ARFI were performed on the uMR790 system since a high amplitude DEG is required to have enough sensitivity. The maximum gradient amplitude of uMR790 can reach as high as 100mT/m. A small 800 kHz single element focused ultrasound transducer (Imasonics, Besancon, France), whose focal length was 5 cm and active diameter was 4 cm, was used for image registration validation and transcranial MR-ARFI. The electrical to acoustical efficiency of this transducer is 80%. While for all the other experiments, a more prominent 800 kHz single element focused ultrasound transducer (Imasonics, Besancon, France), whose focal length was 10 cm and active diameter was 12 cm, was used. The electrical to acoustical efficiency of the transducer was 65%. An arbitrary waveform generator (33220A, Agilent Technologies, Santa Clara, CA, USA) was used to generate sine waves. A customer-designed 55dB power amplified the sine waveform to drive the transducer.

B. Coordinate Registration and Validation

An ultrasound transducer holder with four localizer balls was specially designed for coordinate registration. The localize balls were filled with 1.5% gadolinium solution and distributed on the holder with their exact coordinates ($U_{x,k}, U_{y,k}, U_{z,k}$) in U-coordinate known as a priori. A 3D MP-RAGE scan with 0.5mm $\times$ 0.5mm $\times$ 0.5mm resolution was first performed to find the localizer balls. The geometric focal point of the transducer in the image coordinate was then determined based on (2). The accuracy of the transducer focus registration was validated by a heating experiment to see whether the calculated ultrasound focus coincided with the heating spot. The heating experiments were performed three times in the *ex vivo* pork muscle, and the 2D temperature image data were acquired in all the three orthogonal planes around the ultrasound focus. The input electric power of the HIFU transducer was set to 7.5W. Temperature measurements during the continuous HIFU sonication were obtained using a 2D GRE sequence. TE/TR = 10ms/29ms, BW = 130Hz/pixel, Resolution = 1.5mm $\times$ 1.5mm $\times$ 1.5mm, Matrix = 128 $\times$ 128, Flip angle =10°. Ten slices without spacing were scanned in each imaging orientation.

C. Focus Localization Based on MR-ARFI

MR-ARFI based on the spin-echo sequence was first compared with the predicted geometric focus and the heating experiments in *ex vivo* porcine muscle. The instantaneous electrical power for MR-ARFI experiment was set to 55W. The FUS pulse was triggered by the transistor-transistor logic (TTL) signal generated by the MR sequence and synchronized to the DEG. The pulse length of HIFU was 21.76 ms, which would cause little thermal effect. The interleaved acquisition of φ^+, φ^-, and φ^+_{ref}, φ^-_{ref} was used to reduce the motion artefacts and the duty cycle of the HIFU pulse. The direction of DEG was always parallel to the ultrasound waveform. The imaging parameters were: TE/TR = 43ms/600ms, BW = 500Hz/pixel, Resolution = 1.5mm × 1.5mm × 5.0 mm, Matrix = 128 × 128, the amplitude of DEG = 75 mT/m, with duration τ = 15 ms.

D. Temperature and Thermal Dose Measurement

The temperature measurement was first carried out in *ex vivo* porcine muscle. A 2D RF spoiled GRE sequence was performed to monitor the temperature change in the sagital plane. The evaluation of the temperature monitoring accuracy was presented in Appendix D of Supplementary Materials. The imaging parameters were: TE/TR = 10ms/ 29ms, BW = 190Hz/pixel, Resolution = 1.5mm × 1.5mm × 3.0mm, Matrix = 128 × 128, Flip angle = 10°. An 8-channel flex coil was used for data acquisition. The baseline temperature of 22°C (The room temperature) was used for thermal dose calculation. The accuracy of the thermal dose that was calculated by the software during sonication was evaluated by comparing the size of the denatured tissue after sonication with such calculations.

E. Motion Correction

Motion correction for temperature imaging was validated in a healthy volunteer's liver with free-breathing. No obvious temperature change was expected. A segmented 2D gradient-echo EPI sequence (2D-EPI) with water excitation was measured 180 times. A sagittal slice of liver was scanned with the imaging parameters: TE/TR =10ms/25ms, BW = 1085Hz/Pixel, Resolution = 1.5mm × 1.5mm × 8.0mm, Matrix = 192 × 156, Flip angle = 10°, EPI factor = 11. A 12 channel body coil was used for signal detection. The temperature change (average over 25 pixels) with a single reference and multi references were compared. For multi-reference monitoring with PCA motion correction [24], the first 20 images formed the reference atlas, while the temperature change in the other images was continuously monitored.

F. Temperature Control

The temperature control was tested *in vivo* on a rabbit thigh. The rabbit was anaesthetized by isoflurane and fixed in a water coupling plate above the water tank. The rabbit thigh was shaved before the experiment. The temperature rise target was set to 5°C, and the imaging parameters were the same as that used for the real-time-temperature measurement. An ARMA (3, 3) model was adopted for the closed-loop temperature control. The initial 18 measurements with random small controller outputs were used for system identification to obtain the initial guess of the model. The Diophantine equation [26] was used in iterative optimization for the synthesis of feedback control systems, allowing the temperature to rise to the targeted value quickly and avoid overshoots.

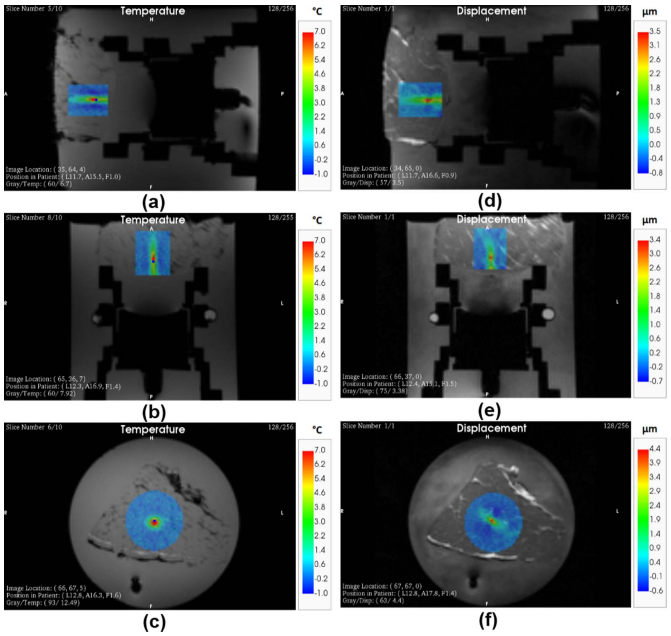

Fig. 7. (a-c) The heating experiment of MR registration. The red dot represents the pixel experience of the max temperature change. The blue dot represents the position of the predicted geometric focus. (d-f). The MR-ARFI results of focus localization.

G. Transcranial MR-ARFI of Monkey

MR-ARFI was then performed in a monkey to verify the transcranial focus localization. The monkey was placed in an MR stereotaxic frame and anaesthetized with isoflurane. The hair on the skull was shaved and coupled with degassed water. The input electrical power was set to 170W for the ARF generation. The imaging parameters were: TE/TR = 45ms/1000ms, BW = 500Hz/pixel, Resolution = 2.0mm × 2.0mm × 5.0mm, Matrix = 64 × 64, the amplitude of DEG = 84mT/m, with duration τ = 15ms. A customer-designed single coil was placed close to the monkey skull, providing high SNR images in all three orientations.

IV. Results

A. Coordinate Registration

The temperature and displacement maps in all the three orthogonal planes are shown in Fig. 7. The most critical issue at the pre-treatment planning stage was to locate the focus of the ultrasound wave precisely. In the temperature map, the hottest pixel was marked as a red dot, while the predicted focus based on coordinate registration was marked as a blue dot. The predicted geometric focus of the transducer was (L12.6, A16.1, F1.1), while the focus determined by

TABLE I
THE FOCAL POINT DETERMINED BY IMAGING REGISTRATION, HEATING AND MR-ARFI EXPERIMENTS

	Image registration	Heating experiment	Differences (mm)	ARFI experiments	Differences (mm)
Coronal	(L12.6, A16.1, F1.1)	(L12.8, A16.3, F1.6)	(0.2, 0.2,0.5)	(L12.8, A17.8, F1.4)	(0.2, 1.7, 0.3)
Transversal	(L12.6, A16.1, F1.1)	(L12.3, A16.9, F1.4)	(0.3, 0.8, 0.3)	(L12.4, A15.1, F1.5)	(0.2, 0.9, 0.4)
Sagittal	(L12.6, A16.1, F1.1)	(L11.7, A15.5, F1.0)	(0.9, 0.6, 0.1)	(L11.7, A16.6, F0.9)	(0.9, 0.5,0.2)

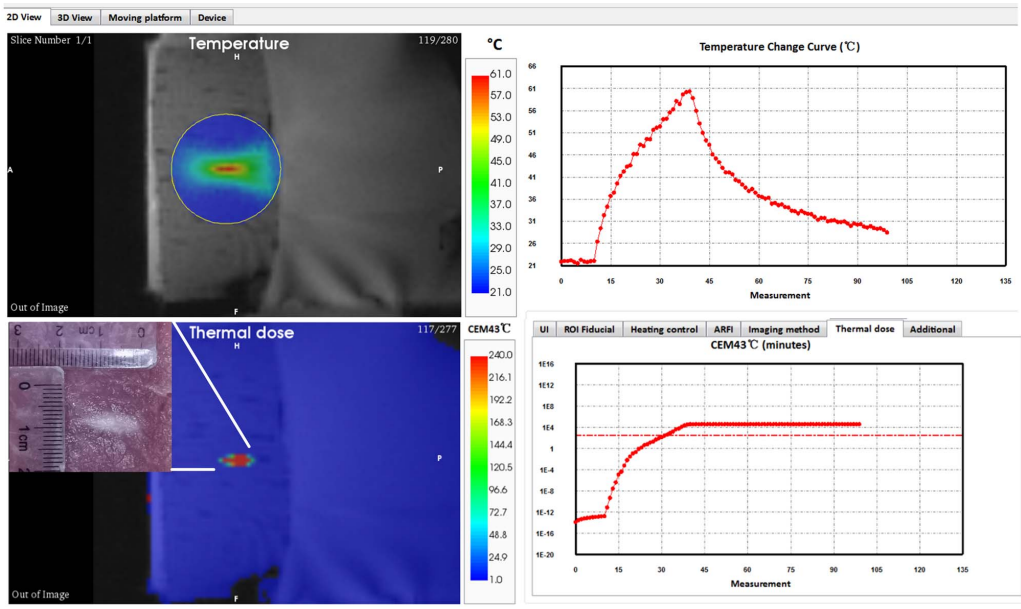

Fig. 8. Temperature monitoring and thermal dose. The inset image showed the sliced muscle after sonication.

heating and ARFI experiments were only slightly biased from the image registration. The determined position of the focus was summarized in Table I. The max difference between the image registration and heating experiment, and the difference between the image registration and MR-ARFI, were both 0.9mm. The results demonstrated that the customer designed holder in conjunction with the image registration algorithm could precisely predict the focus.

B. Temperature Monitoring and Thermal Dose

The temperature monitoring results in *ex vivo* muscle are shown in Fig. 8. The max temperature in focus reached 60.17°C. The thermal dose curve of the focal point was shown in the lower-right corner, in which the dashed line indicated the 240min damage threshold. In the thermal dose map, the region exceeded the damage threshold was labelled in red, and the corresponding sliced image of the muscle was shown in the inserted image. The predicted lethal area in the muscle from the thermal dose map appeared similar to the sliced photo.

C. Motion Correction

The temperature mapping results based on a single pre-scanned baseline image are demonstrated in Fig. 9(a). The temperature monitoring in the liver was challenging due to the respiratory motion. A significant temperature rise was observed in the upper boundary of the liver, even without heating during the volunteer experiment. The 25 points average temperature evolution around the specified pixel was plotted in real-time on the right side of the software. Significant temperature error was noted without appropriate motion correction. The average temperature change reached was 5.56°C, with a standard deviation of 10.73°C. The maximum peak-to-peak change of the temperature during a respiratory cycle was up to 39.89°C. In comparison, the temperature map based on the multi-reference atlas (Fig. 9(b)) effectively decreased the temperature error in the whole liver. The mean and the standard deviation of the temperature change in the same area were only −0.18°C and 0.86°C, respectively.

D. Temperature Control

The temperature control results are illustrated in Fig. 10. The implemented MPC algorithm predicted the desired voltage output to robustly maintain the focus temperature rise at 5°C in a rabbit thigh. The final target temperature reached 42 °C of hyperthermia. The temporal resolution was 2.27s/frame. The computation time for MPC algorithm was much less than the acquisition frame rate. The first 18 measurements after HIFU turned ON was used for system identification. Then the temperature reached the targeted value (42°C, 37°C basal body temperature plus 5°C target value) soon after the system

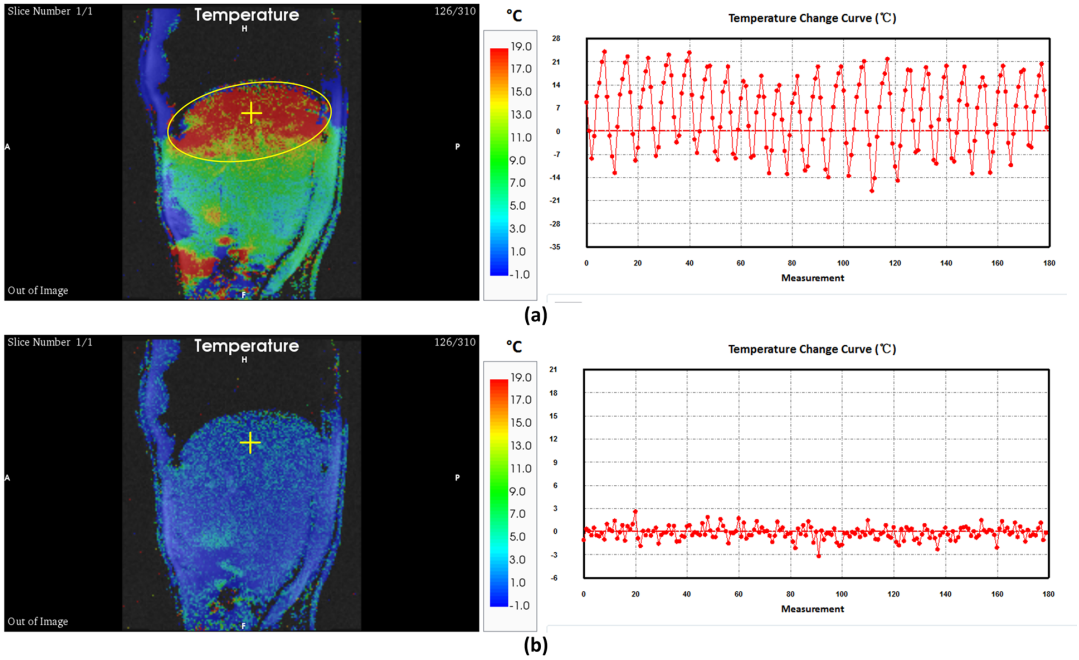

Fig. 9. Temperature monitoring (a) with single reference and (b) with principal component analysis.

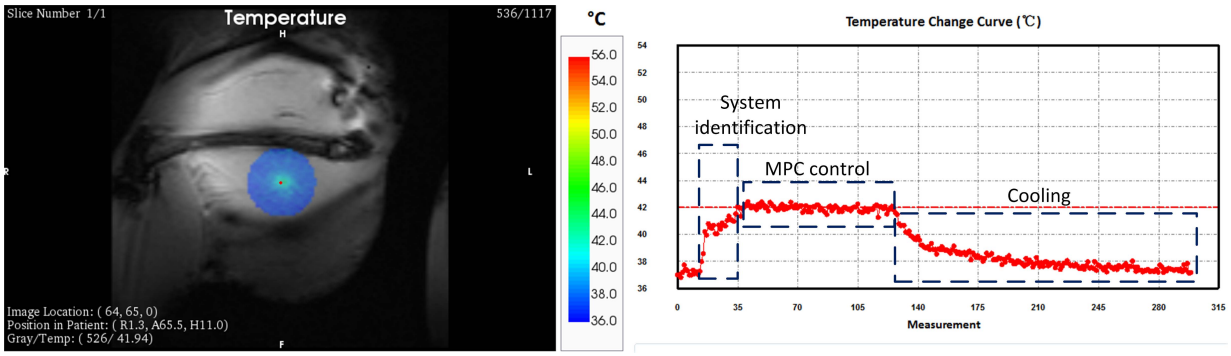

Fig. 10. Illustration of the real-time temperature control results in the rabbit thigh.

identification procedure. No evident overshoot was observed. The average temperature and standard deviation during the MPC control stage from measurement #35 to #125 were 41.89°C and 0.31°C, respectively. The maximum temperature reached was 5.55°C. The temperature curve of the focal point is depicted in Fig. 10.

E. Transcranial Focus Localization

The transcranial focus localization results in coronal and transversal planes are illustrated in Fig. 11. The displacement map was overlaid on the magnitude image. The peak displacement was 1.71 μm in the coronal plane (Fig. 11(a)) and 1.92 μm in the transversal plane (Fig. 11(b)). The coordinates of the corresponding pixel in the two planes were (R1.2, A48.4, F22.5) and (R1.2, A49.1, F24.4), showing high consistency. The blue dots coordinate was (L0.4, A41.5, F22.5), indicating the position of the predicted geometric focus from the coordinate registration. The SNR of the magnitude image in the brain was over 100, making the acquired displacement reliable.

V. Discussion

In this study, we developed an integrated MR guided focused ultrasound monitoring software. The software was validated by many *ex vivo* and *in vivo* experiments and showed promising efficacy for the real-time monitoring of focused ultrasound. All the experiments have been tested in both Siemens and UIH systems except for transcranial MR-ARFI.

To best of our knowledge, the software contains the most comprehensive functions for preclinical MRgFUS such as coordinate registration, ultrasound focus localization, temperature and thermal dose monitoring, motion correction and temperature control. Then the transcranial focus localization experiment was carried out on monkey, which is the most appealing technique in targeting the focus ultrasound for use in neuromodulation [16].

Similarly, Zaporzan *et al.* have developed a platform to communicate with MRI scanner and control of focused ultrasound system. However, the software was only friendly to the users of Philips scanner [11]. Poorman *et al.* have developed

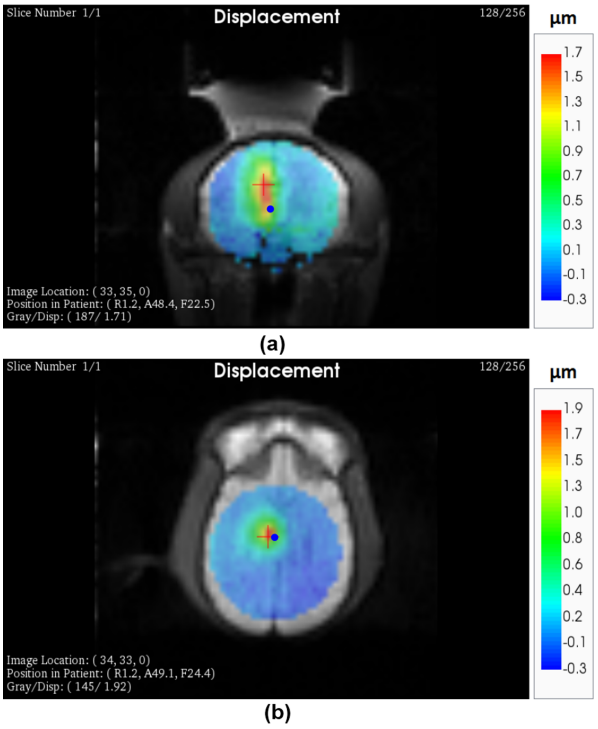

Fig. 11. Transcranial MR-ARFI in (a) coronal and (b) transversal plane. The blue dots indicate the position of the predicted geometric focus.

an open-source, small animal MR guided focused ultrasound system based on Matlab [14]. In comparison, our software was developed based on C++ and worked with the Gadgetron reconstruction framework. The MR data were transferred to the Gadgetron line by line and reconstructed in real-time, which is especially important to monitor information with minimum latency. In addition, Gadgetron also shares a lot of well-predefined image reconstruction algorithm, which can be organized in the Gadgetron pipeline directly, thus, making our software more flexible for real-time applications. For example, the temporal resolution in volumetric MR thermometry which is based on a 3D echo-shifted sequence, can be optimized within 3 seconds [27].

Along with fundamental temperature monitoring and thermal dose calculation, the function of the software was tested in complicated large animals and volunteer studies. *In vivo* transcranial focus localization based on the SE-ARFI was realized with the help of a large DEG gradient and a customer-designed monkey coil. Field drift was corrected with the interleaved acquisition of the reference image. To our knowledge, only a few groups [17], [28]–[30] have utilized *in vivo* MR-ARFI focalization in the large animal due to physiological noise, motion artefacts, and a high requirement of the gradient system. The main disadvantages of SE-ARFI were long acquisition time and the requirement for repeated ultrasound pulses. The software was also compatible with EPI-ARFI as long as the EPI reconstruction pipeline in Gadgetron was invoked.

Respiratory motion is one of the primary sources of the temperature error. With the integrated PCA algorithm, the motion induced phase errors were corrected well. The monitored temperature changes were much closer to the real value zero, and had a much smaller standard deviation. However, this experiment configuration didn't involve real heating *in vivo*. Therefore, other confounding factors for accurate temperature mapping, such as heat induced local field and tissue susceptibility changes, are not considered in the current implementation. Further evaluation with real heating will be carried out in future to complete the validation of motion correction with EPI sequence.

Compared to the traditional PID control algorithm, the MPC controller uses the most recent data to rectify the estimated model parameter and optimizes the outputs in a short future time window iteratively. Also, the MPC algorithm shows more adaptability to different types of tissues and does not need tedious parameter tuning.

The time efficiency of the image processing module was mainly determined by the computer configuration and the algorithm performed. In the current scenarios, the computation time of the post-processing were all less than a second, which may hardly influence the dynamic guidance.

Even though the MARFit software is intended to be suitable for large animal MRgFUS studies, there are still some limitations. As mentioned above, respiration motion correction with actual heating in large animals is needed to fully validate the performance of the motion correction function. For transcranial focus localization, single element ultrasound transducer was used. Thus, phase correction was not considered in the software. A significant difference between the predicted geometric focus and the MR-ARFI focus at the A-P direction was observed, which attributed to the phase aberration caused by the skull. Besides, more animal studies are desired to validate the software.

VI. Conclusion

In this study, we presented an integrated MRgFUS software which can act as a powerful tool for pre-clinical MRgFUS research. MARFit communicating with Gadgetron permits real-time image reconstruction. The post-processing module covers multiple sophisticated MRgFUS applications. The software allows adaptability, extensibility, flexibility and translatability between different vendors of MR system, which can foster collaboration between cross-disciplinary research teams in conducting extensive animal preclinical studies with FUS.

References

[1] W. J. Elias *et al.*, "A pilot study of focused ultrasound thalamotomy for essential tremor," *New England J. Med.*, vol. 369, pp. 640–648, Aug. 2013.
[2] A. Magara, R. Bühler, D. Moser, M. Kowalski, P. Pourtehrani, and D. Jeanmonod, "First experience with MR-guided focused ultrasound in the treatment of Parkinson's disease," *J. Therapeutic Ultrasound*, vol. 2, no. 11, pp. 1–8, 2014.
[3] Y. Meng *et al.*, "Blood-brain barrier opening in Alzheimer's disease using MR-guided focused ultrasound," *Neurosurgery*, vol. 66, pp. 1–8, Sep. 2019.
[4] B. Z. Fite *et al.*, "Magnetic resonance thermometry at 7T for real-time monitoring and correction of ultrasound induced mild hyperthermia," *PLoS ONE*, vol. 7, no. 4, Apr. 2012, Art. no. e35509.
[5] R. Magnin *et al.*, "Magnetic resonance-guided motorized transcranial ultrasound system for blood-brain barrier permeabilization along arbitrary trajectories in rodents," *J. Ther. Ultrasound*, vol. 3, no. 1, p. 22, 2015.

[6] Y. Liu *et al.*, "Concurrent visualization of acoustic radiation force displacement and shear wave propagation with 7T MRI," *PLoS ONE*, vol. 10, no. 10, Oct. 2015, Art. no. e0139667.

[7] J. M. Santos, G. A. Wright, and J. M. Pauly, "Flexible real-time magnetic resonance imaging framework," in *Proc. 26th Annu. Int. Conf. IEEE Eng. Med. Biol. Soc.*, Sep. 2004, pp. 1048–1051.

[8] P. E. Radau *et al.*, "VURTIGO: Visualization platform for real-time, MRI-guided cardiac electroanatomic mapping," in *Proc. STACOM*. Berlin, Germany: Springer, 2011, pp. 244–253.

[9] E. K. Brodsky, W. F. Block, A. L. Alexander, M. E. Emborg, C. D. Ross, and K. A. Sillay, "Intraoperative device targeting using real-time MRI," in *Proc. Biomed. Sci. Eng. Conf., Image Informat. Anal. Biomed.*, Mar. 2011, pp. 1–4.

[10] J. Smink *et al.*, "eXTernal Control (XTC): A flexible, real-time, low-latency, bi-directional scanner interface," in *Proc. ISMRM*, 2011, p. 1755.

[11] B. Zaporzan, A. C. Waspe, T. Looi, C. Mougenot, A. Partanen, and S. Pichardo, "MatMRI and MatHIFU: Software toolboxes for real-time monitoring and control of MR-guided HIFU," *J. Therapeutic Ultrasound*, vol. 1, no. 1, pp. 1–12, Dec. 2013.

[12] B. Rieck, L. Curiel, C. Mougenot, K. Zhang, and S. Pichardo, "Treatment of localized abscesses induced by methicillin-resistant Staphylococcus aureus (MRSA) using MRgFUS: First *in vivo* results," in *Proc. AIP Conf.*, 2012, pp. 173–178.

[13] S. Pichardo *et al.*, "Proteus: A software platform for multisite development of MRI-guided focused ultrasound applications," in *Proc. ISTU*, Nashville, TN, USA, 2018, pp. 137–139.

[14] M. E. Poorman *et al.*, "Open-source, small-animal magnetic resonance-guided focused ultrasound system," *J. Therapeutic Ultrasound*, vol. 4, no. 1, pp. 1–16, Dec. 2016.

[15] M. S. Hansen and T. S. Sorensen, "Gadgetron: An open source framework for medical image reconstruction," *Magn. Reson. Med.*, vol. 69, pp. 1768–1776, Jun. 2013.

[16] N. M. Spivak and T. P. Kuhn, "Variations in targeting techniques of focused ultrasound for use in neuromodulation," *Brain Stimulation*, vol. 12, no. 6, pp. 1595–1596, Nov. 2019.

[17] V. Ozenne *et al.*, "MRI monitoring of temperature and displacement for transcranial focus ultrasound applications," *NeuroImage*, vol. 204, Jan. 2020, Art. no. 116236.

[18] J. Chen, R. Watkins, and K. B. Pauly, "Optimization of encoding gradients for MR-ARFI," *Magn. Reson. Med.*, vol. 63, no. 4, pp. 1050–1058, Apr. 2010.

[19] J. D. Poorter, C. D. Wagter, Y. D. Deene, C. Thomsen, F. Ståhlberg, and E. Achten, "Noninvasive MRI thermometry with the proton resonance frequency (PRF) method: *in vivo* results in human muscle," *Magn. Reson. Med.*, vol. 33, no. 1, pp. 74–81, Jan. 1995.

[20] G. C. van Rhoon, T. Samaras, P. S. Yarmolenko, M. W. Dewhirst, E. Neufeld, and N. Kuster, "CEM43°C thermal dose thresholds: A potential guide for magnetic resonance radiofrequency exposure levels," *Eur. Radiol.*, vol. 23, pp. 2215–2227, Apr. 2013.

[21] P. L. de Oliveira, B. D. de Senneville, I. Dragonu, and C. T. W. Moonen, "Rapid motion correction in MR-guided high-intensity focused ultrasound heating using real-time ultrasound echo information," *NMR Biomed.*, vol. 23, no. 9, pp. 1103–1108, Nov. 2010.

[22] Z. Celicanin *et al.*, "Real-time method for motion-compensated MR thermometry and MRgHIFU treatment in abdominal organs," *Magn. Reson. Med.*, vol. 72, no. 4, pp. 1087–1095, Oct. 2014.

[23] M. O. Köhler, B. D. de Senneville, B. Quesson, C. T. W. Moonen, and M. Ries, "Spectrally selective pencil-beam navigator for motion compensation of MR-guided high-intensity focused ultrasound therapy of abdominal organs," *Magn. Reson. Med.*, vol. 66, no. 1, pp. 102–111, Jul. 2011.

[24] J. Tan, C. Mougenot, S. Pichardo, J. M. Drake, and A. C. Waspe, "Motion compensation using principal component analysis and projection onto dipole fields for abdominal magnetic resonance thermometry," *Magn. Reson. Med.*, vol. 81, no. 1, pp. 195–207, Jan. 2019.

[25] C. Zou, H. Shen, M. He, C. Tie, Y.-C. Chung, and X. Liu, "A fast referenceless PRFS-based MR thermometry by phase finite difference," *Phys. Med. Biol.*, vol. 58, no. 16, pp. 5735–5751, Aug. 2013.

[26] V. Kučera, "Diophantine equations in control—A survey," *Automatica*, vol. 29, no. 6, pp. 1361–1375, Nov. 1993.

[27] R. Jiang *et al.*, "Real-time volumetric MR thermometry using 3D echo-shifted sequence under an open source reconstruction platform," *Magn. Reson. Imag.*, vol. 70, pp. 22–28, Jul. 2020.

[28] M. A. Phipps *et al.*, "Considerations for ultrasound exposure during transcranial MR acoustic radiation force imaging," *Sci. Rep.*, vol. 9, no. 1, p. 16235, Dec. 2019.

[29] P. Gaur *et al.*, "Histologic safety of transcranial focused ultrasound neuromodulation and magnetic resonance acoustic radiation force imaging in rhesus macaques and sheep," *Brain Stimulation*, vol. 13, no. 3, pp. 804–814, May 2020.

[30] V. Chaplin *et al.*, "On the accuracy of optically tracked transducers for image-guided transcranial ultrasound," *Int. J. Comput. Assist. Radiol. Surg.*, vol. 14, no. 8, pp. 1317–1327, Aug. 2019.